

## Noncollinear $XY$ spin system: First-order transition and evidence of a reentrance

E. H. Boubcheur, R. Quartu, and H. T. Diep

*Laboratoire de Physique Théorique et Modélisation, Université de Cergy-Pontoise, 2, Avenue Adolphe Chauvin, 95302 Cergy-Pontoise Cedex, France*

O. Nagai\*

*Department of Physics, Faculty of Science, Kobe University, Kobe 657, Japan*

(Received 9 January 1998)

We study the frustrated  $XY$  model on stacked three-dimensional checkerboard lattices by means of extensive Monte Carlo (MC) calculations. When the system is fully frustrated, the histogram MC results show that the transition is clearly of first order. In a range of parameter of frustration  $\eta$  we find evidence of the reentrance phenomenon. The phase diagram in the  $(\eta, \text{temperature})$  plane is presented and discussed. The quantum version of the model is also studied by a self-consistent Green-function technique. Some results are shown and compared with MC simulations. [S0163-1829(98)02425-4]

### I. INTRODUCTION

In recent years, much effort has been devoted to frustrated spin systems. There are several reasons for this increasing interest. On the one hand, many real systems which show competing interactions cannot be explained by simple model Hamiltonians. An example is planar arrays of coupled Josephson junctions which can be studied by mapping it into a frustrated  $XY$  two-dimensional (2D) model. On the other hand, from a fundamental point of view in statistical physics, in particular in the domain of phase transitions and critical phenomena, frustrated systems are of great interest because they serve as a testing ground for more sophisticated theories and approximations. Among the most controversial subjects, we can mention the nature of the phase transition in noncollinear magnets such as helimagnets and in  $XY$  and Heisenberg stacked antiferromagnetic triangular lattices (SATL). Ten years ago, Kawamura suggested from a renormalization group (RG) calculation and Monte Carlo (MC) simulations that the transition in  $XY$  and Heisenberg models belong each to a new universality class.<sup>1</sup> Soon after, Azaria *et al.*<sup>2</sup> suggested from a nonlinear  $\sigma$  model that if the transition is not of first order or mean-field tricritical then it should be  $O(4)$  universality. Numerical simulations<sup>3-5</sup> did not confirm these conjectures. Antonenko and Sokoloff<sup>6</sup> went further with RG calculations and concluded that the transition is of first order. At the present time, the question remains unsettled.

Another spectacular effect of the frustration is the reentrance phenomenon. In some frustrated 2D Ising exactly solved models, it has been shown that the frustration can give rise to a partial disorder which favors the occurrence of a reentrance, i.e., a disordered phase between two ordered phases on the temperature scale.<sup>7,8</sup> For reviews on various other aspects of frustrated spin systems, the reader is referred to Ref. 9. We note that while partial disorder has been discovered very recently in  $XY$  and Heisenberg systems,<sup>10-12</sup> reentrance has never been found in any non-Ising models.

This paper has been motivated by the above unsettled questions, i.e., the nature of the phase transition and the existence of reentrance in periodically noncollinear  $XY$  spin

systems. Of course, depending on the ground-state (GS) symmetry and the GS degeneracy, noncollinear spin systems may behave differently. The above-mentioned SATL with  $XY$  spins, for example, has twofold degeneracy (Ising-like) while the system studied here has an infinite GS degeneracy as we will see later. Our purpose is not to settle the controversial question of the SATL case, but to show the richness of physical behaviors of noncollinear spin systems to stimulate further theoretical investigations.

The system studied here is a frustrated 3D  $XY$  spin system consisting of planes stacking in the  $Z$  direction. Each plane is a square lattice with one frustrated plaquette every two in two directions (see Fig. 1). We call this model *frustrated checkerboard model*. We use both MC simulations and a Green-function technique, for comparison.

Section II is devoted to the description of the model and its classical GS. In Sec. III, we show the MC results in details. In particular, evidence of first-order transition is found in a region of the phase diagram where the spin configuration of the ordered phase is noncollinear. We recall that previous works also found a first-order transition in frustrated systems,<sup>3,4</sup> but these transitions, except in a  $XY$  helical magnet,<sup>13</sup> occur from a collinear state to the paramagnetic state. Section IV is devoted to a Green-function calculation

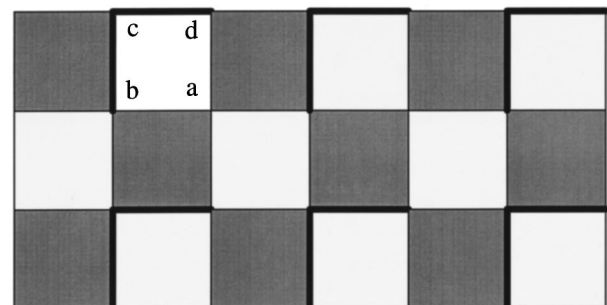


FIG. 1. Checkerboard lattice. Heavy (thin) lines are antiferromagnetic (ferromagnetic) bonds. Frustrated (nonfrustrated) plaquettes are gray (white). The four sublattices are denoted by  $a$ ,  $b$ ,  $c$ , and  $d$ .

performed for quantum  $XY$  spins on the same lattice. Some results are shown and compared with the classical spin results. Concluding remarks are given in the last section.

## II. MODEL AND GROUND STATE

Let us present here the general classical GS of the system. We consider the model shown in Fig. 1 with the following Hamiltonian:

$$H = - \sum_{\langle ij \rangle} J_{ij} \mathbf{S}_i \cdot \mathbf{S}_j, \quad (1)$$

where  $\sum_{\langle ij \rangle}$  indicates the sum over the nearest-neighbor (NN) spin pairs.  $J_{ij}$  denotes the NN exchange coupling. In the  $XY$  planes,  $J_{ij}$  takes two values:  $J > 0$  for ferromagnetic bonds and  $J' = -\eta J$  ( $\eta > 0$ ) for antiferromagnetic bonds. For simplicity, the interaction in the stacking direction  $Z$  is set equal to  $J$ . We shall use  $J$  as a unit of temperature and energy below. The  $J$  bonds are represented by single lines in Fig. 1, and the  $J'$  bonds are represented by heavy lines. Let us call  $a$  spins the spins connected to neighbors only by  $J$  bonds, and  $b$ ,  $c$ , and  $d$  spins the remaining spins (i.e., spins connected to neighbors by both  $J'$  and  $J$  bonds).  $\eta$  can take an arbitrary positive value. When  $\eta = 1$  the system is fully frustrated. To determine the classical GS, it suffices to consider four plaquettes: two frustrated plaquettes (the gray ones in Fig. 1) and two nonfrustrated plaquettes. Once the spin configuration of the frustrated plaquette is determined, one can construct the whole spin configuration of a  $XY$  plane by matching the spin configurations of neighboring plaquettes. Care must be taken to count all the matching possibilities, i.e., the degeneracy. Since the interaction in the stacking direction is ferromagnetic, the same GS configuration is for all  $XY$  planes.

Following Berge *et al.*,<sup>14</sup> we calculate the GS spin configuration of a frustrated plaquette by a variational method (the interaction in the  $Z$  direction does not affect the spin configuration). We find that the cosines of the angles  $\theta_{ij}$  of the spins  $\mathbf{S}_i$  and  $\mathbf{S}_j$  linked by the positive bonds  $J$  are all equal and given by

$$\cos(\theta) = \frac{1}{2} \left[ \frac{\eta + 1}{\eta} \right]^{1/2}, \quad (2)$$

while  $\theta'_{ij}$  of the spins  $\mathbf{S}_i$  and  $\mathbf{S}_j$  linked by the bond  $J'$  are all equal and given by

$$\theta' = 3\theta. \quad (3)$$

The critical value of  $\eta$  is  $\eta = \frac{1}{3}$  above which the GS spin configuration is noncollinear. Note that for each plaquette, the GS configuration is twice degenerate with  $\pm\theta$ , i.e., left chirality (LC) and right chirality (RC).<sup>16</sup> As said earlier, the GS spin configuration of a  $XY$  plane is constructed starting from a configuration of a plaquette. For matching purposes, we show in Fig. 2(a) all left and right chirality configurations. One can distinguish the following GS types: (i) states with the same chirality such as all frustrated plaquettes being of LC or all of RC, for example, a state with sequence  $L_1 L_2 L_3 L_4 \dots$ , (ii) states with LC and RC alternately such as  $L_1 R_1 L_1 R_1 \dots$  [see Fig. 2(b)], (iii) states with periodically

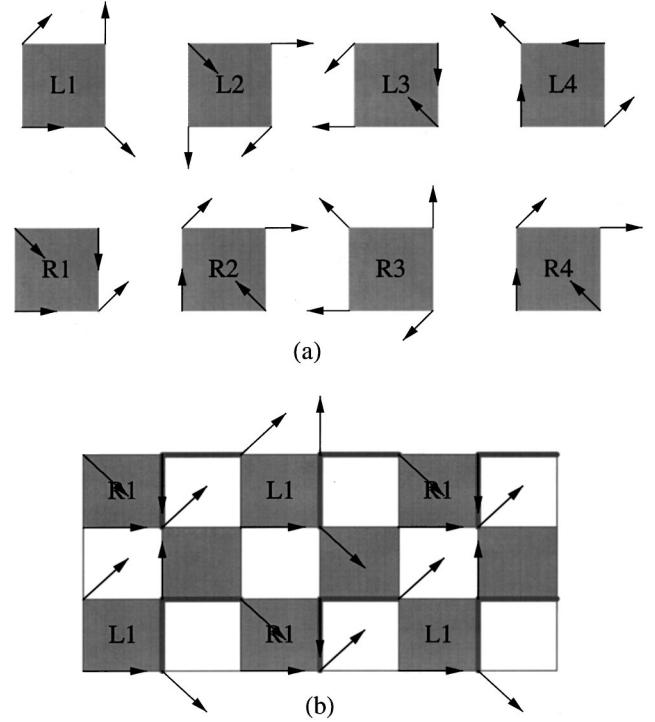


FIG. 2. (a) four left and four right chirality configurations, (b) an example of a GS with alternate chiralities.

mixed chiralities such as the sequence  $L_1 L_2 L_3 L_4 R_4 L_4 \dots$ , (iv) states with randomly mixed chiralities (matching is, however, necessary). One can easily check that the degeneracy is larger than  $2^{\sqrt{N}/2}$ , i.e., infinite in the thermodynamic limit. We note that the GS energy per plaquette of the ferromagnetic phase is given by  $U_0 = (\eta - 3)/2 - 1$  for  $\eta \leq \frac{1}{3}$ , while that of the noncollinear (frustrated) phase ( $\eta \geq \frac{1}{3}$ ) is given by

$$U_0 = -\frac{1}{2} \frac{(1 + \eta)^{3/2}}{\eta^{1/2}} - 1.$$

## III. MONTE CARLO SIMULATIONS

Our model has been obtained by stacking the 2D configurations shown in Fig. 2. We have performed both standard and histogram MC simulations using the sample sizes of  $N = L^3$  spins where  $L = 12$  up to 44 for various values of  $\eta$ . The largest size has been used to calculate the energy histogram  $P(E)$  ( $E$  is the system energy) as well as other physical quantities as functions of temperature  $T$ .

Since the GS configuration is either commensurate or incommensurate (random mixing of chiralities), we can use periodic boundary conditions only for system sizes commensurate with GS configurations shown in Fig. 2(b). Note that for  $\eta = 1$  the linear size should be a multiple of 4. In the case where the angle  $\theta$  is not commensurate with the lattice size within a reasonable value of  $L$ , we use the so-called ‘‘fluctuating boundary conditions.’’<sup>15</sup> In each run, we have discarded about 20 000 MC steps per spin before averaging physical quantities over the next 80 000 MC steps per spin (MCS) in standard MC calculations. Histogram MC calculations have been carried over  $2 \times 10^6$  MCS.

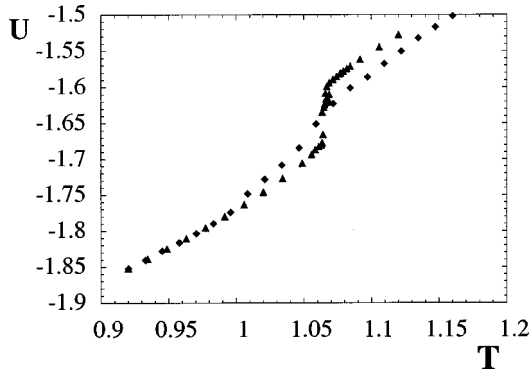


FIG. 3. Internal energy per spin  $U$  versus  $T$  in the case  $\eta=1$  for two extreme lattice sizes studied  $12^3$  (diamonds) and  $44^3$  (triangles) are shown. The jump at the transition is seen only with the large size.

### A. The case of $\eta=1$

When  $\eta=1$ , we have found a single transition with a first-order character as shown by the curve  $U$  (energy per spin) versus  $T$  in Fig. 3. Note that the jump of  $U$  is observed only with a very large lattice size. We show in Fig. 4 the magnetization defined by  $M = \langle \sum_i |\mathbf{S}_i| / N \rangle$ , where  $\mathbf{S}_i$  is the  $i$ th sublattice total spin and the angular brackets indicating the thermal average. One defines the chirality order parameter as

$$K = \frac{1}{N} \sum_p (-1)^p \sum_{\langle ij \rangle} (\mathbf{S}_i \times \mathbf{S}_j)_p, \quad (4)$$

where  $p$  indicates the frustrated plaquette. The parity  $(-1)^p$  is chosen according to the GS symmetry. If a GS with the same chirality is chosen, then the parity is 1. The chirality order parameter is also shown in Fig. 4. The first-order character of the transition is confirmed by the histogram MC simulation shown below.

In order to confirm the nature of the transition when  $\eta = 1$ , we use the histogram MC technique which was devel-

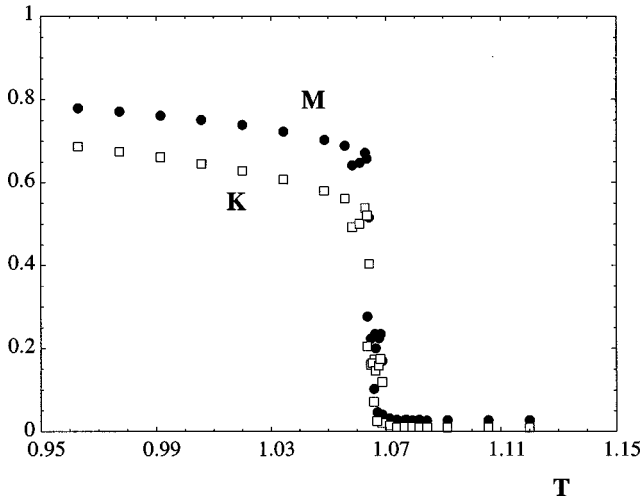


FIG. 4. Magnetization  $M$  (black circles) and chirality order parameter  $K$  (white squares) versus  $T$  are shown near the transition, for  $\eta=1$  with lattice size  $44^3$ . See text for the definition of  $M$  and  $K$ . They are normalized by their values at  $T=0$ .

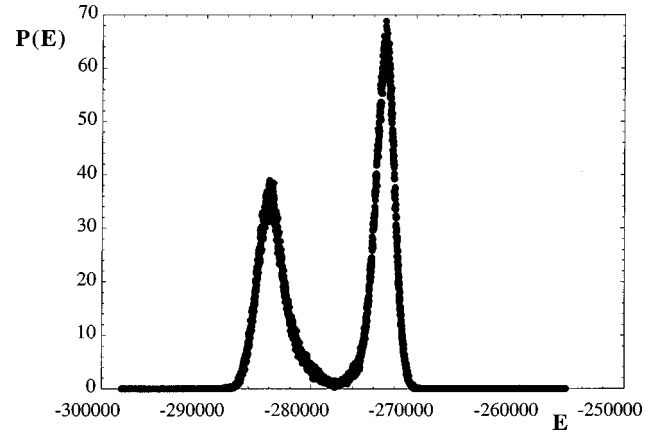


FIG. 5. Bimodal distribution of the total internal energy  $P(E)$  for  $\eta=1$  at the transition indicating a first-order transition.

oped by Ferrenberg and Swendsen.<sup>17,18</sup> We use systems of  $N=44^3$  spins with periodic boundary conditions. We first estimate as precisely as possible the “transition” temperature  $T_0$  at  $L=44$  and then performed at  $T_0$  the energy histogram  $P(E)$  ( $E$  being the total energy) over  $2 \times 10^6$  MC steps per spin after discarding  $10^6$  MC steps per spin for equilibrating the system. The result is shown in Fig. 5 where two peaks are observed at  $T_0=1.06378$ . This bimodal distribution of energy at the transition is a clear evidence of the first-order character of the transition suggested above.

At this stage, it is worth mentioning that a first-order transition has been suggested by MC simulation in a number of frustrated vector spin systems such as stacked triangular antiferromagnets,<sup>3,4</sup> hcp (Ref. 19) and fcc (Ref. 20) antiferromagnets, and bct  $XY$  helimagnets.<sup>13</sup> However, except for the last case, the first-order transition was suggested in the phase region where a collinear spin configuration is the ordered phase (in the mentioned  $XY$  bct case,<sup>13</sup> a first-order transition was suggested from a standard MC simulation). Therefore, we emphasize that a first-order transition is firmly found for the transition from a noncollinear configuration to the paramagnetic state. This has some fundamental importance since this shows that the question of the nature of the phase transition in helimagnets mentioned in the Introduction cannot be solved as long as one cannot identify the ingredient which governs the transition. The infinite GS degeneracy of the present system may play an important role in the very clear first-order character of the transition, unlike in the stacked triangular antiferromagnet.

Let us note that though the GS is infinitely degenerate, the system prefers to choose states with *the same chirality* (all left or all right) at finite  $T$ . It is noted that if one heats the system from a random or a mixed-chirality GS, it is only near the phase transition that the system will be ordered with the same chirality. It means that at low  $T$ , there may be some finite barriers between different kinds of ordering symmetry in the phase space. These barriers disappear near the transition. We show in Fig. 6(a) a chirality snapshot below the transition. Only one kind of chirality is seen though the system is heated from the GS with mixed LC and RC. Cooling the system from high  $T$ , we also get a state with the same chirality below the transition (note, however, that cooling to

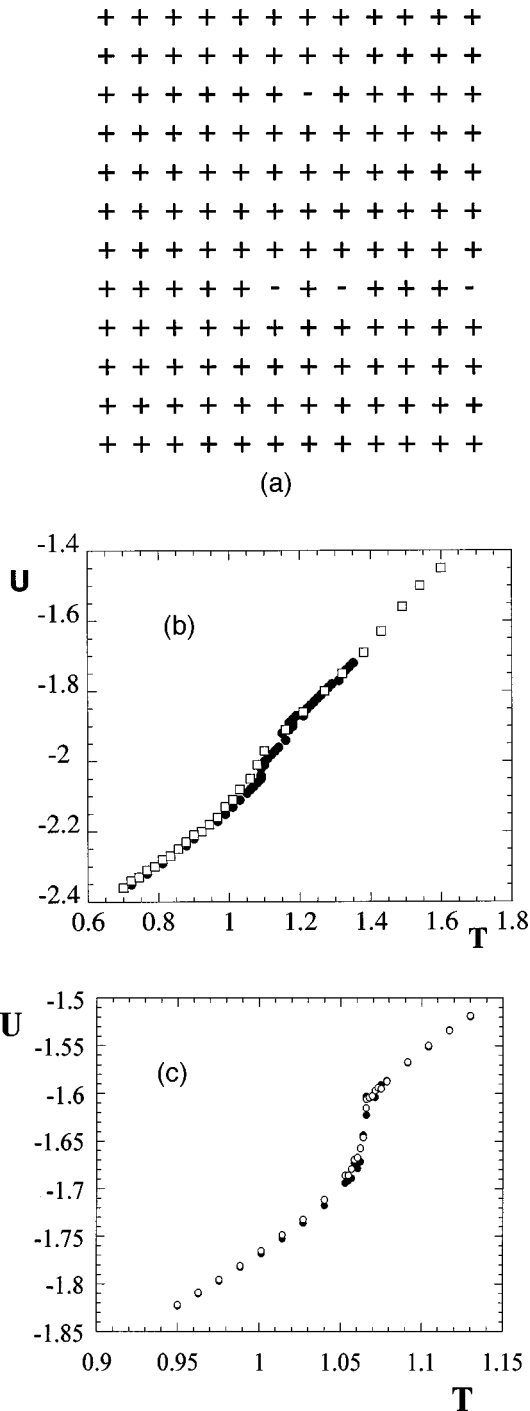


FIG. 6. (a) Chirality snapshot at  $T=1$  for  $\eta=1$ : one observes the same chirality ordering, although the system is heated from a GS with mixed left and right chiralities. (b) Internal energy per spin  $U$  versus  $T$  for  $\eta=1.7$  with mixed LR chiralities (black circles) and all  $L$  chirality (squares) ( $L=24$ ). See text for comments. (c) Internal energy per spin  $U$  versus  $T$  for  $\eta=1$  with mixed LR chiralities (black circles) and all  $L$  chirality (void circles) ( $L=24$ ).

very low  $T$  results in metastable states as expected since the relaxation time is very long). As a last remark, let us emphasize that the internal energy versus  $T$  shown in Figs. 6(b) and 6(c) for  $\eta=1.7$  and  $\eta=1$  does not change significantly with different initial conditions, so the preference of the system for a symmetry of the same chirality at finite  $T$  results certainly from an entropy effect.

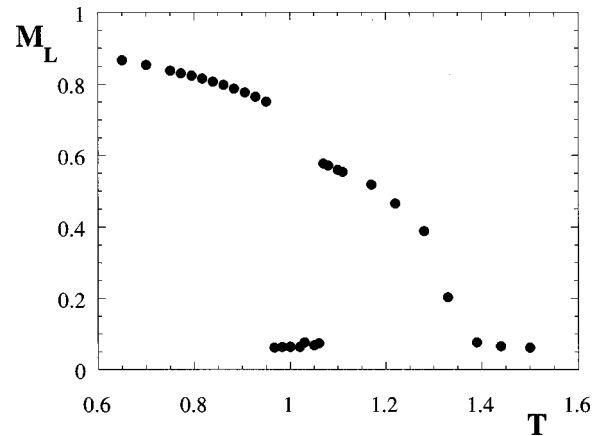


FIG. 7. Local magnetization  $M_L$  versus  $T$  where  $\eta=0.618$  ( $\theta=36^\circ$ ).  $M_L$  is defined as  $M_L = \sum_i \langle |S_i| \rangle / N$ , where  $S_i$  is the total spin of the sublattice containing parallel spins in the GS. There are two ordered phases with a reentrant phase in between. See text for comment.

### B. $\eta \neq 1$

When  $\eta \neq 1$ , there may be several transitions for a given set of parameters. Figure 7 shows an example where  $\eta=0.618$  ( $\theta=36^\circ$ ). The local magnetization vanishes in a very narrow range of temperature  $T=0.95-1.07$  and goes up again before vanishing at a higher temperature  $T=1.35$ . This remarkable behavior provides evidence that the system is disordered in a low- $T$  interval and becomes ordered again up to some higher  $T$ . The low- $T$  disordered phase is called the *reentrant phase* (a reentrant phase can be defined as a phase with no long-range order, or no order at all, occurring in a region between two ordered phases on the temperature scale). This is a very important finding since the reentrance phase has recently been found for some 2D frustrated Ising spin systems,<sup>7-9</sup> but has never been observed in a vector spin system.

The low- $T$  ordered phase is the noncollinear state and the high- $T$  ordered phase is ferromagnetic. This is shown in Fig.

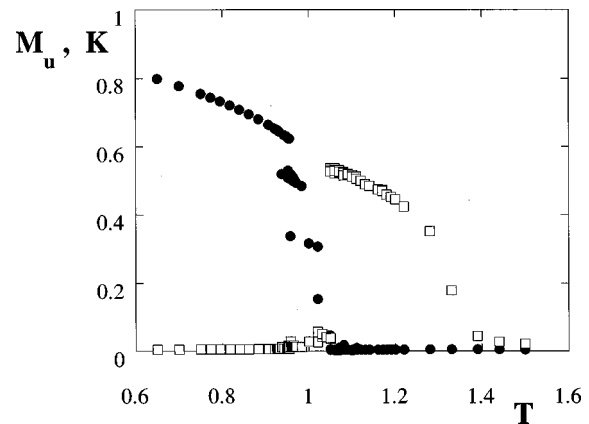


FIG. 8. Chirality order parameter  $K$  (black circles) characterized the low- $T$  noncollinear ordering and total uniform magnetization  $M_u$  characterized the high- $T$  ferromagnetic phase (squares) versus  $T$  for  $\eta=0.618$ ,  $L=40$ .  $M_u$  is defined as  $M_u = \langle |\sum_i S_i| \rangle$  where  $S_i$  is the  $i$ th spin.  $M_u$ , zero in the low- $T$  phase because of the helimagnetic structure, shows a jump while entering the high- $T$  ferromagnetic phase.  $K$  is normalized by its value at  $T=0$ .

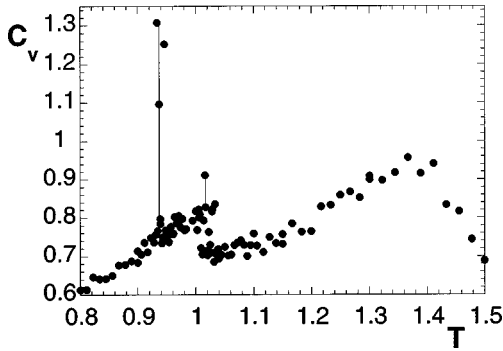


FIG. 9. Specific heat versus  $T$  for  $\eta=0.618$  ( $L=40$ ). Two low- $T$  peaks are highlighted by vertical lines. See text for comments.

8, where  $\eta=0.618$ : the chirality order parameter is well defined at low  $T$  while the uniform (total) magnetization (zero at low  $T$  due to the noncollinear structure) shows a jump at high  $T$ , indicating that the ordering is a ferromagnetic state.

We show in Fig. 9 the specific heat versus  $T$  calculated by energy fluctuations. In spite of the narrowness of the reentrant region, it is possible to see the two low- $T$  peaks. Thus, the existence of the reentrant region, clearly seen by the local magnetization (Fig. 7), can also be seen in the specific heat.

Now, when  $\eta$  is rather large, one also observes a similar behavior, namely, a reentrant region between two ordered phases. The sublattice magnetizations are shown in Fig. 10 for  $\eta=1.7$ . One sees that the center-spin sublattice ( $a$ ) becomes disordered at low  $T$  while the other three sublattices ( $b$ ,  $c$ , and  $d$ ) remain ordered up to a higher  $T$ . The high- $T$  ordered phase, called the *partially ordered phase*, is due to the fact that the antiferromagnetic bonds are much stronger than the ferromagnetic bonds in this region ( $\eta$  is much larger than 1). Note that the partial order in other frustrated vector spin systems has been recently observed.<sup>10-12</sup> This phenomenon seems now to be a general effect in frustrated vector spin systems whenever anisotropic interactions are present. The specific heat is shown in Fig. 11 for  $\eta=1.7$  where we observe a well separation of the two peaks at low  $T$  which limits the reentrant region.

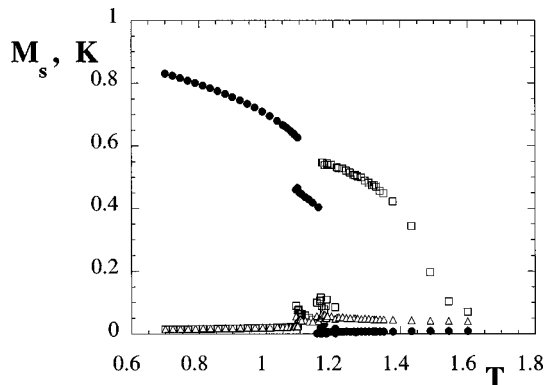


FIG. 10. Chirality  $K$  (black circles) and sublattice magnetizations  $M_s$  versus  $T$  for  $\eta=1.7$ .  $M_s$  is defined as  $M_s = \langle |\sum_i \mathbf{S}_i| / N/4 \rangle$  where  $\mathbf{S}_i$  is the  $i$ th spin belonging to one sublattice. Squares correspond to sublattices  $b$ ,  $c$ , and  $d$  (indistinguishable) while triangles show the  $a$  sublattice magnetization. Note that all sublattice magnetizations are zero at low  $T$  due to the noncollinear structure of each sublattice (not disordering). At high  $T$  the sublattice  $a$  becomes disordered while others remain ordered (partially disordered phase) up to paramagnetic phase.

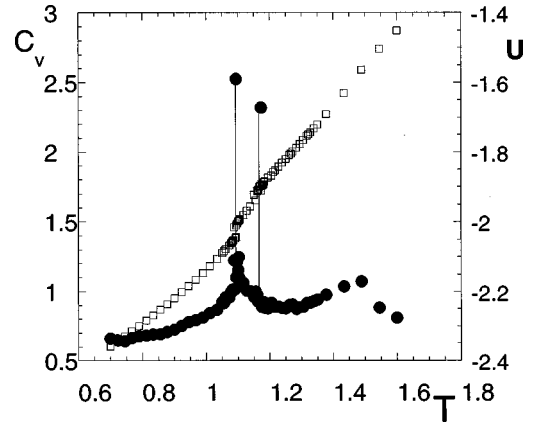


FIG. 11. Specific heat  $C_v$  (black circles, left scale) and internal energy per spin  $U$  (squares, right scale) versus  $T$  for  $\eta=1.7$  ( $L=24$ ). Two low- $T$  peaks are highlighted by vertical lines.

Calculations have been performed for the whole range of  $\eta$ . Whenever the angle  $\theta$  is not compatible with the lattice size we use the fluctuating boundary conditions<sup>15</sup> as said earlier. We display in Fig. 12 the phase diagram in the plane ( $T, \eta$ ). In this diagram we can see four regions: the ferromagnetic phase (I), the noncollinear phase (II), the partially ordered (PO) phase (III), and the paramagnetic phase (P).

Let us discuss now the nature of ordering at low  $T$  in different regions of the phase diagram (Fig. 12). As in the case where  $\eta=1$  shown above, we find, by starting with different kinds of initial GS's, that the system always chooses an ordered state with the same chirality at finite  $T$  everywhere in the noncollinear phase (II). This is very similar to the so-called order by disorder introduced by Villain *et al.*<sup>21</sup> for frustrated Ising spin systems.

#### IV. QUANTUM RESULTS

Let us show the results for the quantum spin case. Using the Green-function method presented below, we have calculated self-consistently various physical quantities as function of temperature  $T$ . A size of  $20^3$  points in the first Brillouin zone has been used.

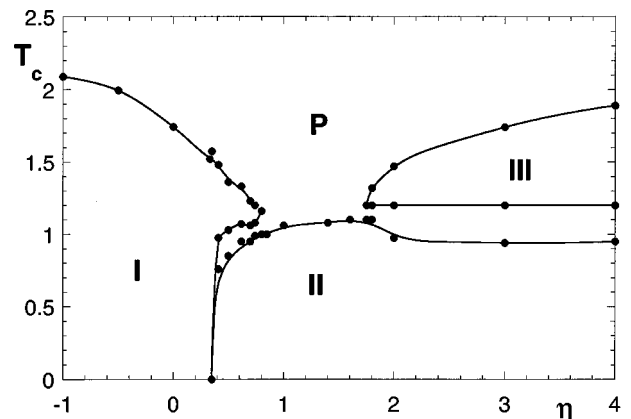


FIG. 12. Phase diagram in the plane ( $\eta, T_c$ ). There are four regions: the ferromagnetic phase (I), the noncollinear phase (II), the partially ordered (PO) phase (III), and the paramagnetic phase (P). See text for comments.

### A. Method

Let us present here the general formalism that can be applied to the general case where the spins are either Heisenberg or  $XY$  type with general spin magnitude. Application to the  $XY$  case is given in the next section. We consider a model system described by the Hamiltonian (1). The classical GS is planar and its energy per spin is given by

$$U_c = \frac{J}{4} S_c (S_b + S_d) [\cos(\theta_2) + \eta \cos(\theta_3) + 2\epsilon \cos(\theta_1)] + \frac{J_v}{4} (S_a^2 + S_b^2 + S_c^2 + S_d^2) \cos(\theta_v), \quad (5)$$

where  $\epsilon = S_a/S_c$  and  $\theta_2$  is the angle between a  $b$  spin and a  $c$  spin or a  $c$  spin and a  $d$  spin. While  $\theta_3$  is the angle between a spin  $b$  and a spin  $c$  of the neighboring plaquette or between a spin  $c$  and a spin  $d$  of the neighboring plaquette,  $\theta_1$  is the angle between the spins  $a$  and  $b$  or between  $a$  and  $d$ . Note that  $\theta_v$ , the angle between spins belonging to adjacent basal planes, is always equal to 0. The relation between the angles is given by

$$\cos(\theta_1) = \frac{1}{2} \left[ \frac{\epsilon^2(\eta+1)^2}{(\eta+\epsilon^2)\eta} \right]^{1/2},$$

$$\sin(\theta_2) = -\epsilon \sin(\theta_1),$$

$$\theta_3 = \theta_2 - 2\theta_1. \quad (6)$$

We shall use the Green-function method to calculate the energy, magnetization, angles, and other thermodynamic quantities as functions of temperature. The details of the method have been given in Ref. 10. We briefly recall it here and show the application to the present model.

For numerical calculations we have used a small stabilizing field  $d$  pointing in the local quantization axis at each site (see Ref. 10 for a discussion on its effect). We note that the local  $z$ -axis direction can change with the temperature upon iteration.<sup>10</sup>

We can rewrite the Hamiltonian in the local framework<sup>22</sup> as

$$H = 2 \sum_{\langle kl \rangle} \frac{1}{4} J_{kl}^- (S_k^+ S_l^+ + S_k^- S_l^-) + \frac{1}{4} J_{kl}^+ (S_k^+ S_l^- + S_k^- S_l^+) + J_{kl}^z \cos(\beta_{kl}) S_k^z S_l^z + 2 \sum_i d_i S_i^z, \quad (7)$$

where  $\beta_{kl}$  is the angle between the two spins at the lattice sites  $k$  and  $l$  and

$$J_{kl}^\pm(\beta_{kl}) = \pm J_{kl}^x + J_{kl}^y \cos(\beta_{kl}), \quad (8)$$

where we have decomposed the interaction  $J_{kl}$  into  $J_{kl}^x$ ,  $J_{kl}^y$ ,  $J_{kl}^z$ . For the spins linked by a  $J$  bond,  $J_{kl}^\sigma = J^\sigma$  ( $\sigma = x, y, z$ ) and for the spins linked by a  $J'$  bond,  $J_{kl}^\sigma = J'^\sigma$  ( $\sigma = x, y, z$ ). For the planar spin model, one puts one of these components equal to zero, and the other two are taken to be the same. Since we define the local quantization axis as the  $z$  axis of the spins, the case of planar spins will correspond to  $J_{kl}^x = 0$ .

Following Tahir-Kheli and ter Haar,<sup>23</sup> we define two double-time Green functions for each pair of spins. For our lattice, we need eight such Green functions. Then, we write the equations of motion for them, neglecting higher-order correlations by using the Tyablikov decoupling scheme. The Fourier transforms of the Green functions  $g^+$  and  $g^-$  satisfy a set of equations which can be rewritten under the matrix form  $\Delta(E)\mathbf{g} = \mathbf{u}$ , where

$$\Delta(E) = \begin{pmatrix} E+Q_a & -\lambda_{ab}^+ & -\lambda_{ad}^+ & 0 & -Z_a^- & -\lambda_{ab}^- & -\lambda_{ad}^- & 0 \\ -\lambda_{ba}^+ & E+Q_b & 0 & -\lambda_{bc}^+ & -\lambda_{ba}^- & -Z_b^- & 0 & -\lambda_{bc}^- \\ -\lambda_{da}^+ & 0 & E+Q_d & -\lambda_{dc}^+ & -\lambda_{da}^- & 0 & -Z_d^- & -\lambda_{dc}^- \\ 0 & -\lambda_{cb}^+ & -\lambda_{cd}^+ & E+Q_c & 0 & -\lambda_{cb}^- & -\lambda_{cd}^- & -Z_c^- \\ Z_a^- & \lambda_{ab}^- & \lambda_{ad}^- & 0 & E-Q_a & \lambda_{ab}^+ & \lambda_{ad}^+ & 0 \\ \lambda_{ba}^- & Z_b^- & 0 & \lambda_{bc}^- & \lambda_{ba}^+ & E-Q_b & 0 & \lambda_{bc}^+ \\ \lambda_{da}^- & 0 & Z_d^- & \lambda_{dc}^- & \lambda_{da}^+ & 0 & E-Q_d & \lambda_{dc}^+ \\ 0 & \lambda_{cb}^- & \lambda_{cd}^- & Z_c^- & 0 & \lambda_{cb}^+ & \lambda_{cd}^+ & E-Q_c \end{pmatrix},$$

$$\mathbf{g} = \begin{pmatrix} g_{a\delta}^+ \\ g_{b\delta}^+ \\ g_{d\delta}^+ \\ g_{c\delta}^+ \\ g_{a\delta}^- \\ g_{b\delta}^- \\ g_{d\delta}^- \\ g_{c\delta}^- \end{pmatrix}, \quad \mathbf{u} = \begin{pmatrix} u_a(n) \delta_{a,\delta} \\ u_b(n) \delta_{a,\delta} \\ u_d(n) \delta_{a,\delta} \\ u_c(n) \delta_{a,\delta} \\ 0 \\ 0 \\ 0 \\ 0 \end{pmatrix}, \quad (9)$$

$$Z_i^\pm = 2J_v^\pm \mu_i \cos(K_z), \quad i=(a,b,c,d), \quad (10)$$

$$\lambda_{ab}^\pm = 2J^\pm(\theta_1) \mu_a \cos(K_x),$$

$$\lambda_{ad}^\pm = 2J^\pm(\theta_1) \mu_a \cos(K_y),$$

$$\lambda_{ba}^\pm = 2J^\pm(\theta_1) \mu_b \cos(K_x),$$

$$\lambda_{da}^\pm = 2J^\pm(\theta_1) \mu_d \cos(K_y),$$

$$\lambda_{cd}^\pm = \mu_c [J^\pm(\theta_2) e^{-iK_x} + J'^\pm(\theta_3) e^{iK_x}],$$

$$\lambda_{cb}^\pm = \mu_c [J^\pm(\theta_2) e^{iK_y} + J'^\pm(\theta_3) e^{-iK_y}],$$

$$\lambda_{dc}^\pm = \mu_d [J^\pm(\theta_2) e^{iK_x} + J'^\pm(\theta_3) e^{-iK_x}],$$

$$\lambda_{bc}^\pm = \mu_b [J^\pm(\theta_2) e^{-iK_y} + J'^\pm(\theta_3) e^{iK_y}],$$

$$Q_a = 2[2J_z \cos(\theta_1) \mu_b + 2J_z \cos(\theta_1) \mu_d + 2J_{vz} \cos(\theta_v) \mu_a + d_a] - Z_a^+,$$

$$Q_b = 2[2J_z \cos(\theta_1) \mu_a + J_z \cos(\theta_2) \mu_c + J' z \cos(\theta_3) \mu_c + 2J_{vz} \cos(\theta_v) \mu_b + d_b] - Z_b^+,$$

$$Q_d = 2[2J_z \cos(\theta_1) \mu_a + J_z \cos(\theta_2) \mu_c + J'_z \cos(\theta_3) \mu_c + 2J_{vz} \cos(\theta_v) \mu_d + d_d] - Z_d^+,$$

$$Q_c = 2[J_z \cos(\theta_2) \mu_b + J_z \cos(\theta_2) \mu_d + J'_z \cos(\theta_3) \mu_b + J'_z \cos(\theta_3) \mu_d + 2J_{vz} \cos(\theta_v) \mu_c + d_c] - Z_c^+, \quad (11)$$

where  $\mu_i = \langle S_i^z \rangle$  ( $i=a,b,c,d$ ),  $\langle \dots \rangle$  being the thermal average.

Solving numerically these equations, we obtain the spin-wave spectrum of the present system. Next, using the spectral theorem which relates the correlation function  $\langle S_i^{-n} S_j^{+n} \rangle$  to the Green functions.<sup>24</sup> For the details on how to determine  $\langle S_i^{-n} S_j^{+n} \rangle$ , the reader is referred to Ref. 10.

The internal energy per atom  $U$  is given by taking the thermal average value of the Hamiltonian. As in Ref. 10, we use a mean-field-like approximation to obtain the angles: they are calculated by minimizing  $U$ , instead of the free energy. The relations obtained, in the first-order approximation in  $\langle S^\pm S^\pm \rangle$ , is the same as that of Eq. (5) but with

$$\epsilon = \frac{\langle S_a^+ S_b^- + S_a^+ S_d^- + S_a^- S_b^- + S_a^- S_d^- \rangle + \langle S_a^z \rangle \langle S_b^z \rangle + \langle S_a^z \rangle \langle S_d^z \rangle}{\langle S_c^+ S_b^- + S_c^+ S_d^- + S_c^- S_b^- + S_c^- S_d^- \rangle + \langle S_c^z \rangle \langle S_b^z \rangle + \langle S_c^z \rangle \langle S_d^z \rangle}. \quad (12)$$

The specific heat is obtained by taking numerical derivative of  $U$  with respect to  $T$ .

### B. Quantum effect on the angles

The three angles  $\theta_2$ ,  $\theta_3$ , and  $\theta_1$  are modified by quantum fluctuations in the noncollinear phase. Quantum effect sets in for  $\eta \geq \frac{1}{3}$ . The classical relations  $\theta_2 = \theta_1 = \theta_3/3 = \theta_c$  and  $\cos(\theta_c) = \frac{1}{2}[(\eta+1)/\eta]^{1/2}$  are true only for  $\eta = 1$ . For other values we have the following.

(i) For  $\frac{1}{3} < \eta < 0.39$ , the three angles obtained are equal to zero at any  $T$  showing that the collinear state is favored by quantum fluctuations causing a shift from the classical critical value  $\eta = 1/3$  to 0.39. This is the so-called ‘‘order by disorder’’ due to quantum fluctuations.<sup>25</sup>

(ii) For  $0.4 \leq \eta \leq 0.5$ , the three angles have, at  $T=0$ , values smaller than the corresponding classical ones. When  $T$  increases the values of the angles decrease and change abruptly to zero at the transition.

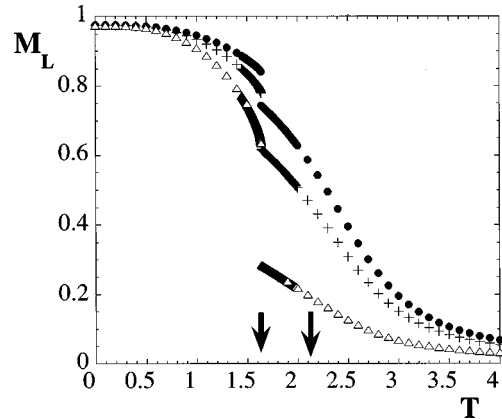


FIG. 13. Quantum case: Local order parameters  $M_L$  versus  $T$  for  $\eta = 0.618$ . Triangles, crosses, and black circles correspond, respectively, to sublattices  $c$ ,  $b$ , and  $a$ . Sublattice  $d$  coincides with sublattice  $b$ . Arrows indicate transition temperatures. See text for comments.

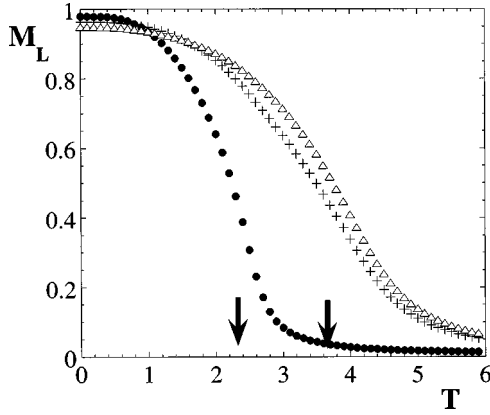


FIG. 14. Quantum case: Local order parameters  $M_L$  versus  $T$  for  $\eta=4$ . Triangles, crosses, and black circles correspond, respectively, to sublattices  $c$ ,  $b$ , and  $a$ . Sublattice  $d$  coincides with sublattice  $b$ . Arrows indicate transition temperatures. See text for comments.

(iii) For  $0.6 \leq \eta < 1$  we have  $\theta_2 > \theta_{2c}$ ,  $\theta_1 < \theta_{1c}$ , and  $\theta_3 < \theta_{3c}$ . When  $T$  increases  $\theta_1$  and  $\theta_3$  decrease while  $\theta_2$  first increases and then decreases. At the transition the angle values change abruptly to zero.

(iv) For  $\eta=1$  the three angles are equal to the classical values at any  $T$ .

(v) for larger values of  $\eta$ , we have  $\theta_2 < \theta_{2c}$ ,  $\theta_1 > \theta_{1c}$ , and  $\theta_3 > \theta_{3c}$ . When  $T$  increases  $\theta_2$  tends to 0,  $\theta_1$  to  $\pi/2$ , and  $\theta_3$  to  $\pi$ .

(vi) For infinite values of  $\eta$ , we have  $\theta_2=0$ ,  $\theta_1=\pi/2$ , and  $\theta_3=\pi$ .

Quantum fluctuations together with thermal fluctuations affect thus the values of the angles of the classical GS.

### C. Phase transition in the quantum case

We show now the results for the case  $S_a=S_b=S_c=S_d=1$ ,  $J=1$ , and  $d=-0.05$  with varying  $\eta$ . Let us show first an example where  $\eta=0.618$ . In the classical spin case shown above, there are two ordered phases. This is also found in the quantum case. Figure 13 shows the local sublattice magnetizations versus  $T$ . Note, however, that our method does not give the reentrant phase at low temperatures as found in MC simulations shown above. The narrowness of the reentrant phase together with approximations used in the Green-function technique are believed to be one possible cause of the absence of the reentrant phase. Another cause that one cannot exclude is the fact that quantum fluctuations may close the reentrant region observed in the classical case. This question for the quantum case thus remains open.

When  $\eta$  is large, one also observes a partially disordered phase as in the classical case. Figure 14 shows the local magnetizations versus  $T$  for  $\eta=4$ . The partial disorder is seen by the vanishing magnetization of the center spins magnetization at low  $T$ .

We show in Fig. 15 the specific heat versus  $T$  for  $\eta=0.618$  and 4. One sees two peaks for each case. For  $\eta=0.618$ , the low- $T$  one corresponds to the sharp transition from the noncollinear state to the collinear state, while the high- $T$  one corresponds to the transition from the latter to the paramagnetic state. For  $\eta=4$ , the first peak corresponds to

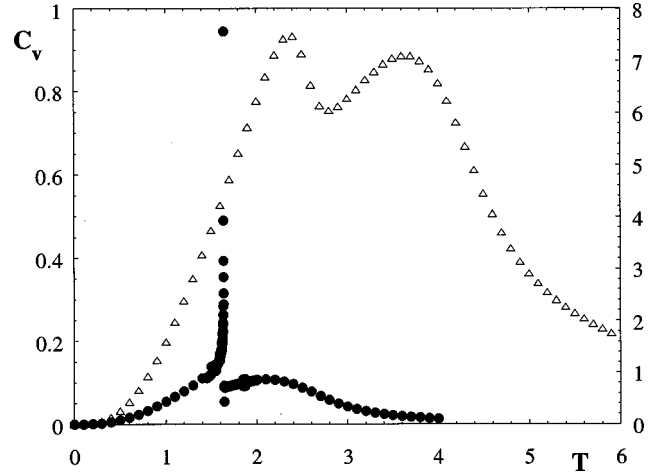


FIG. 15. Quantum case: Specific heat versus  $T$  for  $\eta=0.618$  (black circles) and  $\eta=4$  (triangles). Scale for the black circles (triangles) is on the right (left).

the transition from the frustrated to partially disordered phase, and the second from the latter to the paramagnetic state.

The whole general quantum phase diagram needs much more calculations which are outside the scope of this work. We leave these for the future.

## V. CONCLUSION

We studied in this paper a frustrated XY spin system in three dimensions. Monte Carlo simulations performed for the case of classical XY spins show three striking results.

(i) The first-order transition in the fully frustrated case was clearly demonstrated; this result means that there is no rule yet for the nature of the phase transition in periodically noncollinear spin systems (including helimagnets), some of them exhibit first-order transition,<sup>19,20,13</sup> others show a second-order transition unknown universality class.<sup>1,3,4</sup> There is a need to identify the ingredient which governs the nature of the transition.

(ii) Evidence of the existence of a reentrant phase was found in a vector spin system. This is an important finding since it was believed for a long time that such a phase cannot exist in non-Ising spin systems. Therefore, one must be very careful while interpreting experimental data because of the narrowness of the reentrant phase on the temperature scale.

(iii) A partial disorder in vector spin systems recently observed was again confirmed here.

Finally, we emphasize that the quantum version of the model confirms the existence of two ordered phases for small  $\eta$  and a partially ordered phase above the noncollinear phase for large  $\eta$ . The fact that the quantum version studied by our method does not yield the reentrant phase may be either an effect of the shortcoming of the method or a real physical effect due to quantum fluctuations. This open problem is the subject of future investigation.

## ACKNOWLEDGMENTS

“Laboratoire de Physique Théorique et Modélisation” is an “equipe postulante” (EP 0127) of CNRS.

- \*Present address: Toneyama 2-5-5, Toyonaka 560, Japan.
- <sup>1</sup>H. Kawamura, J. Appl. Phys. **63**, 3086 (1988); J. Phys. Soc. Jpn. **58**, 584 (1989); Phys. Rev. B **38**, 4916 (1988); J. Phys. Soc. Jpn. **61**, 1299 (1992); in *Recent Advances in Magnetism of Transition Metal Compounds*, edited by A. Kotani and Suzuki (World Scientific, Singapore, 1992).
- <sup>2</sup>P. Azaria, B. Delamotte, and Th. Jolicoeur, Phys. Rev. Lett. **64**, 3175 (1990); J. Appl. Phys. **69**, 6170 (1991); P. Azaria, B. Delamotte, F. Delduc, and Th. Jolicoeur, Nucl. Phys. B **408**, 485 (1993).
- <sup>3</sup>D. Loison and H.T. Diep, Phys. Rev. B **50**, 16 453 (1994); T. Bhattacharya, A. Billoire, R. Lacaze, and Th. Jolicoeur, J. Phys. I **4**, 122 (1994).
- <sup>4</sup>E.H. Boubcheur, D. Loison, and H.T. Diep, Phys. Rev. B **54**, 4165 (1996).
- <sup>5</sup>A. Dobry and H. T. Diep, Phys. Rev. B **51**, 6731 (1995); D. Loison and H. T. Diep, J. Appl. Phys. **76**, 6350 (1994).
- <sup>6</sup>S. A. Antonenko and A. I. Sokolov, Phys. Rev. B **49**, 15 901 (1994).
- <sup>7</sup>P. Azaria, H. T. Diep, and H. Giacomini, Phys. Rev. Lett. **59**, 1629 (1987).
- <sup>8</sup>H. T. Diep, M. Debauche, and H. Giacomini, Phys. Rev. B **43**, 8759 (1991), and references therein.
- <sup>9</sup>For recent reviews, see, *Magnetic Systems with Competing Interactions (Frustrated Spin Systems)*, edited by H.T. Diep (World Scientific, Singapore, 1994).
- <sup>10</sup>R. Quartu and H.T. Diep, Phys. Rev. B **55**, 2975 (1997); J. Magn. Mater. **182**, 38 (1998).
- <sup>11</sup>C. Santamaria and H. T. Diep, J. Appl. Phys. **81**, 5276 (1997).
- <sup>12</sup>C. Santamaria, R. Quartu, and H.T. Diep (unpublished).
- <sup>13</sup>H. T. Diep, Phys. Rev. B **39**, 397 (1989).
- <sup>14</sup>B. Berge, H. T. Diep, A. Ghazali, and P. Lallemand, Phys. Rev. B **34**, 3177 (1986).
- <sup>15</sup>W. M. Saslow, M. Gabay, and W.-M. Zhang, Phys. Rev. Lett. **68**, 3627 (1992); P. Olsson, *ibid.* **73**, 3339 (1994).
- <sup>16</sup>J. Villain, J. Phys. C **10**, 1717 (1977).
- <sup>17</sup>A. M. Ferrenberg and R. H. Swendsen, Phys. Rev. Lett. **61**, 2635 (1988).
- <sup>18</sup>A. M. Ferrenberg and R. H. Swendsen, Phys. Rev. Lett. **63**, 1195 (1989).
- <sup>19</sup>H. T. Diep, Phys. Rev. B **45**, 2863 (1992).
- <sup>20</sup>H. T. Diep and H. Kawamura, Phys. Rev. B **40**, 7019 (1989).
- <sup>21</sup>J. Villain, R. Bideaux, J.P. Carton, and R. Conte, J. Phys. (Paris) **41**, 1263 (1980).
- <sup>22</sup>P. Azaria, J. Phys. C **19**, 2773 (1985).
- <sup>23</sup>R. A. Tahir-Kheli and D. ter Haar, Phys. Rev. **172**, 88 (1962).
- <sup>24</sup>D. N. Zubarev, Sov. Phys. JETP **3**, 320 (1960).
- <sup>25</sup>C. L. Henley, J. Appl. Phys. **61**, 3962 (1987); Phys. Rev. Lett. **62**, 2056 (1989).